Monthly Notices of the ROYAL ASTRONOMICAL SOCIETY

MNRAS **447,** 160–167 (2015) doi:10.1093/mnras/stu2439

The Seyfert 2 galaxy NGC 2110: hard X-ray emission observed by *NuSTAR* and variability of the iron Kα line

A. Marinucci,[1⋆] G. Matt,[1] S. Bianchi,[1] T. N. Lu,[2] P. Arevalo,[3,4] M. Baloković,[2] D. Ballantyne,[5] F. E. Bauer,[3,6] S. E. Boggs,[7] F. E. Christensen,[8] W. W. Craig,[8,9] P. Gandhi,[10] C. J. Hailey,[11] F. Harrison,[2] S. Puccetti,[12,13] E. Rivers,[2] D. J. Walton,[2] D. Stern[14] and W. Zhang[15]

[1]*Dipartimento di Matematica e Fisica, Università degli Studi Roma Tre, via della Vasca Navale 84, I-00146 Roma, Italy*
[2]*Cahill Center for Astronomy and Astrophysics, California Institute of Technology, Pasadena, CA 91125 USA*
[3]*Instituto de Astrofísica, Facultad de Física, Pontificia Universidad Católica de Chile, Casilla 306, Santiago 22, Chile*
[4]*Instituto de Física y Astronomía, Facultad de Ciencias, Universidad de Valparaíso, Gran Bretana N 1111, Playa Ancha, Valparaíso, Chile*
[5]*Center for Relativistic Astrophysics, School of Physics, Georgia Institute of Technology, Atlanta, GA 30332, USA*
[6]*Space Science Institute, 4750 Walnut Street, Suite 205, Boulder, CO 80301, USA*
[7]*Space Science Laboratory, University of California, Berkeley, CA 94720, USA*
[8]*DTU Space National Space Institute, Technical University of Denmark, Elektrovej 327, DK-2800 Lyngby, Denmark*
[9]*Lawrence Livermore National Laboratory, Livermore, CA 94550, USA*
[10]*Department of Physics, University of Durham, South Road, Durham, DH1 3LE, UK*
[11]*Columbia Astrophysics Laboratory, Columbia University, New York, NY 10027, USA*
[12]*ASDC-ASI, Via del Politecnico, I-00133 Roma, Italy*
[13]*INAF Osservatorio Astronomico di Roma, via Frascati 33, I-00040 Monte Porzio Catone (RM), Italy*
[14]*Jet Propulsion Laboratory, California Institute of Technology, 4800 Oak Grove Drive, Pasadena, CA 91109, USA*
[15]*NASA Goddard Space Flight Center, Greenbelt, MD 20771, USA*

Accepted 2014 November 15. Received 2014 October 29; in original form 2014 September 15

ABSTRACT

We present *NuSTAR* observations of the bright Seyfert 2 galaxy NGC 2110 obtained in 2012, when the source was at the highest flux level ever observed, and in 2013, when the source was at a more typical flux level. We include archival observations from other X-ray satellites, namely *XMM–Newton*, *Suzaku*, *BeppoSAX*, *Chandra* and *Swift*. Simultaneous *NuSTAR* and *Swift* broad-band spectra (in the 3–80 keV range) indicate a cutoff energy $E_c > 210$ keV, with no detectable contribution from Compton reflection. NGC 2110 is one of the very few sources where no evidence for distant Compton-thick scattering is found and, by using temporal information collected over more than a decade, we investigate variations of the iron Kα line on time-scales of years. The Fe Kα line is likely the sum of two components: one constant (originating from distant Compton-thick material) and the other one variable and linearly correlated with the source flux (possibly arising from Compton-thin material much closer to the black hole).

Key words: galaxies: active – galaxies: individual: NGC 2110 – galaxies: Seyfert.

1 INTRODUCTION

The X-ray spectra of Seyfert 2 galaxies offer a unique opportunity to probe the circumnuclear environment of active galactic nuclei (AGN). The obscuration of the primary radiation by matter with column densities typically in the 10^{22}–10^{24} cm^{-2} range allows a study of the cold and ionized reflectors that cannot be observed, due to dilution effects, in unobscured sources. Typical X-ray features of the cold circumnuclear material include an intense Fe Kα line at 6.4 keV due to fluorescence emission and a reflection continuum peaking at ∼30 keV (George & Fabian 1991; Matt, Perola & Piro 1991).

The primary continuum is thought to arise from the innermost regions surrounding the central black hole, in a hot corona above the accretion disc. It is observed as a power-law spectrum extending to energies determined by the electron temperature in the hot corona (Rybicki & Lightman 1979). The power-law index is a function of the plasma temperature T and optical depth τ.

NGC 2110, at a redshift $z = 0.008$, is one of the brightest Seyfert galaxies in the hard X-ray (>10 keV) band and it shows a prominent Fe Kα line accompanied by variable intrinsic emission (Mushotzky

⋆E-mail: marinucci@fis.uniroma3.it

1982; Hayashi et al. 1996). It has been intensively studied by most X-ray observatories, and it has shown very interesting and peculiar characteristics. Malaguti et al. (1999) reported a photon index of $\Gamma = 1.86$ analysing *BeppoSAX* PDS data above 13 keV (consistent with typical values found in Seyfert 1 sources: Nandra & Pounds 1994). However, when 2–10 keV data are considered, the photon index becomes flatter($\Gamma = 1.67$) and the authors suggested the presence of obscuring material with a column density $N_{\rm H} = 4.1^{+0.5}_{-0.3} \times 10^{22}$ cm^{-2} along the line of sight and an additional absorber with $N_{\rm H} \sim 3 \times 10^{23}$ cm^{-2}, partially covering the nuclear source. This scenario was confirmed by *XMM–Newton*, *Chandra* and *Suzaku* observations (Reeves et al. 2006; Evans et al. 2007; Rivers et al. 2014).

NGC 2110 is one of the very few Seyfert galaxies that, despite the intense iron Kα emission line at 6.4 keV, does not show any Compton reflection from circumnuclear material: values of $R \leq 0.17$ and 0.1 were found with *BeppoSAX* and *Suzaku*, respectively (Malaguti et al. 1999; Rivers et al. 2014). If the line emitting material is Compton thick ($N_{\rm H} > 10^{24}$ cm^{-2}), the iron Kα emission would be accompanied by a Compton reflection component above 10 keV (George & Fabian 1991; Matt et al. 1991). The inferred upper limits on the reflection fraction R in this source suggest that the iron Kα line is not produced by distant, Compton-thick material but is instead emitted by Compton-thin matter, such as in the case of NGC 7213 (Bianchi et al. 2003, 2008).

Recently, *NuSTAR* observed NGC 2110 in an extremely bright state. The lack of reflection components in NGC 2110 arising from the accretion disc or from the putative torus above 10 keV makes this source a perfect candidate for measuring a high-energy cut-off. We present a detailed multi-epoch X-ray study of NGC 2110 including two recent *NuSTAR* observations, obtained in 2012 and 2013, with the dual aims of studying the behaviour of the Fe Kα line with respect to the highly variable intrinsic continuum and of constraining the high-energy cutoff in this source.

2 OBSERVATIONS AND DATA REDUCTION

2.1 *NuSTAR*

NuSTAR (Harrison et al. 2013) observed NGC 2110 with its two coaligned X-ray telescopes with corresponding focal planes: focal plane module A (FPMA) and B (FPMB) starting on 2012 October 5 and 2013 February 14 for a total of ∼32 and ∼26 ks of elapsed time, respectively. The level 1 data products were processed with the *NuSTAR* Data Analysis Software (NUSTARDAS) package (v. 1.3.0). Cleaned event files (level 2 data products) were produced and calibrated using standard filtering criteria with the NUPIPELINE task and the latest calibration files available in the *NuSTAR* calibration data base (CALDB). Both extraction radii for the source and background spectra were 1.5 arcmin. After this process, the net exposure times for the two observations were 15 and 12 ks, with 3–80 keV count rates of 6.53 ± 0.02 and 4.50 ± 0.02 cts s^{-1} for FPMA, and 6.32 ± 0.02 and 4.25 ± 0.02 cts s^{-1} for FPMB. The two pairs of *NuSTAR* spectra were binned in order to oversample the instrumental resolution by at least a factor of 2.5 and to have a signal-to-noise ratio (SNR) greater than 5σ in each spectral channel.

2.2 *Suzaku*

NGC 2110 was observed by *Suzaku* starting on 2005 September 16 (OBSID 100024010) and seven years later, starting on 2012 August 31 (OBSID 707034010). Data were taken from the X-ray Imaging Spectrometer (XIS) and the Hard X-ray Detector (HXD). We reprocessed the event files with the latest calibration files available (2014-02-03) using FTOOLS 6.14 and SUZAKU software Version 21, adopting standard procedures and recommended screening criteria. The source extraction radius was 1.8 arcmin. Background spectra were extracted from source-free regions of 1.8 arcmin radius. Response matrices and ancillary response files were generated using XISRMFGEN and XISARFGEN. The 0.5–10 keV spectra extracted from the front-illuminated XIS0 and XIS3 were co-added using the ftool ADDASCASPEC, for net exposure times of 102 and 103 ks for the two data sets. Spectra were binned in order to oversample the instrumental resolution by at least a factor of 3 and to have no less than 30 counts in each background-subtracted spectral channel. This allows the applicability of χ^2 statistics.

We reduced the HXD PIN data using the AEPIPELINE reprocessing tool, and for background determination we downloaded and utilized the tuned non-X-ray background provided by the HXD team. We extracted source and background spectra using the same good time intervals.

2.3 *XMM–Newton*

NGC 2110 was observed by *XMM–Newton* (Jansen et al. 2001) for ∼60 ks, starting on 2003 March 5 (OBSID 0145670101) with the EPIC CCD cameras, the Pn (Strüder et al. 2001) and the two MOS (Turner et al. 2001), operated in large window and thin filter mode. Data from the MOS detectors are not included in our analysis due to the lower statistics of the spectra. The extraction radii and the optimal time cuts for flaring particle background were computed with SAS 13 (Gabriel et al. 2004) via an iterative process which leads to a maximization of the SNR, similar to the approach described in Piconcelli et al. (2004). The resulting optimal extraction radius was 38 arcsec and the background spectra were extracted from source-free circular regions with a radius of about 50 arcsec.

After this process, the net exposure time was 44 ks for the EPIC-Pn. Spectra were binned in order to oversample the instrumental resolution by at least a factor of 3 and to have no less than 30 counts in each background-subtracted spectral channel.

2.4 *Swift*

There were nine *Swift*/XRT observations of NGC 2110, in 2006, 2008, 2009, 2012 and 2013. The first eight observations were carried out with the photon counting (PC) mode, while the last observation was in window timing (WT) mode (Table 1). ObsIDs 80364001 and 80364002 are simultaneous with *NuSTAR*. We reprocessed all the

Table 1. Observation log for the *Swift* monitoring of NGC 2110. Observations IDs, dates and net exposure times (after filtering and correction for photon pile-up) are reported. Asterisks indicate observations simultaneous with *NuSTAR*.

Obs. ID	Date	$T_{\rm exp}$ (ks)
35459001	2006-03-25	8.3
35459002	2006-04-08	9.2
35459003	2006-04-15	2.3
35459004	2008-08-31	2.2
35459005	2009-10-12	3.5
80364001*	2012-10-05	7.1
35459006	2013-02-03	14.1
80364002*	2013-02-15	0.9
35459007	2013-03-09	2.7

data sets to generate cleaned event files with the XRTPIPELINE script included in the HEASOFT version 6.13. The PC mode observations are all affected by pile-up, while the final observation, obtained in WT mode, does not have pile-up issues. To correct the pile-up, we extracted the source spectrum within a 72 arcsec radius circular region, excluding the central 10 arcsec radius aperture for the PC mode data sets. Obs. IDs, dates and net exposure times are listed in Table 1.

2.5 *Chandra*

NGC 2110 was observed by *Chandra* on 2000-04-22 with the Advanced CCD Imaging Spectrometer (ACIS-S) camera (Obs. ID 883), on 2001-12-19 with three consecutive High Energy Transmission Grating (HETGs) pointings (Obs. ID 3143, 3417 and 3418) and on 2003-03-05 with the HETGs (Obs. ID 4377). All these observations are discussed in detail in Evans et al. (2007) where the four HETG spectra were merged. Since pile-up was found in the ACIS-S observation, we do not use this spectrum in our analysis. Data were reduced using CIAO 4.5 and the latest CALDB files, and we merged Obs. IDs 3143, 3417 and 3418 spectra using the ADD_GRATING_ORDER and ADD_GRATING_SPECTRA tools. The resulting exposure times are 105 and 95 ks for the 2001 and 2003 HETGs data, respectively. Data were binned to have no less than 30 counts in each spectral channel.

2.6 *BeppoSAX*

The source was observed by *BeppoSAX* on 1997-10-12 with the Medium Energy Concentrator Spectrometer (MECS) for a net exposure time of 76 ks. Reduced data were downloaded from the *BeppoSAX* online data archive.[1]

3 SPECTRAL ANALYSIS

We first study the simultaneous *NuSTAR* and *Swift* data to probe the primary radiation from the AGN and the properties of the hot corona. We then perform a multi-epoch phenomenological X-ray analysis to study the behaviour of the Fe Kα emission line in response to variability of the nuclear continuum.

In previous work, broad-band analyses of some data sets revealed the presence of extranuclear emission in the softer ($E<1$ keV) part of the spectra (Evans et al. 2006, 2007; Reeves et al. 2006; Rivers et al. 2014); the analysis of this component is beyond the scope of this work. We focus our analysis on the 3–79 keV band where the contribution from soft diffuse emission is negligible.

The adopted cosmological parameters are $H_0 = 70\,\mathrm{km\,s^{-1}\ Mpc^{-1}}$, $\Omega_\Lambda = 0.73$ and $\Omega_\mathrm{m} = 0.27$, i.e. the default ones in XSPEC 12.8.1 (Arnaud 1996). Errors correspond to the 90 per cent confidence level for one interesting parameter ($\Delta\chi^2 = 2.7$), if not stated otherwise.

3.1 *NuSTAR* 3–80 keV spectral analysis

The X-ray spectra of NGC 2110 have been widely studied in the past few years and several analyses have shown the presence of a $\Gamma \sim 1.7$ power-law continuum partially covered by several layers of absorbing material with column densities in the range 2–6 $\times\ 10^{22}$ cm^{-2} (Evans et al. 2007; Rivers et al. 2014). Above 10 keV, the effect of this absorbing material can be neglected and we therefore start our spectral analysis fitting the *NuSTAR* spectra in the 10–80 keV range, to have a direct measurement of the photon index of the primary power law. We will test a posteriori if this assumption is correct.

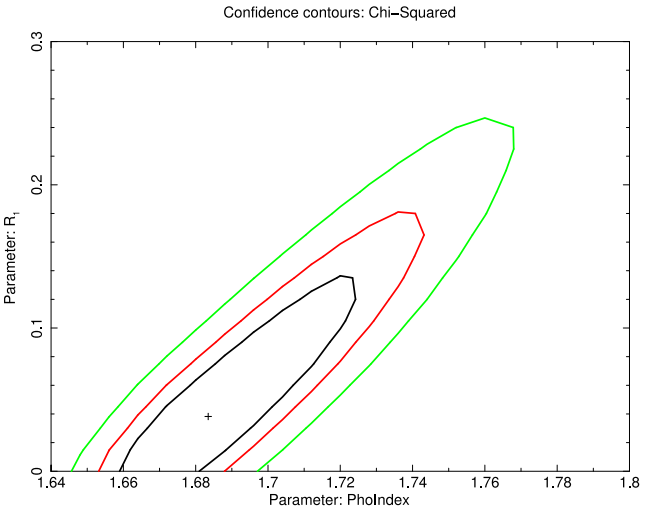

Figure 1. Contour plot between reflection fraction R and photon index Γ for the high-flux *NuSTAR* observation in 2012, when only 10–80 keV data are considered. The solid black, red and green lines correspond to 68, 90 and 99 per cent confidence levels, respectively.

Our model is composed of a power law, with the only free parameters in the fit being the photon index, the normalization of the power law and the cross-calibration factors between the FPMs. When the model is applied to the *NuSTAR* 2012 and 2013 spectra, the fit is good (χ^2/dof=568/601=0.95) and no strong residuals are present across the whole energy band. The best-fitting photon index is $\Gamma = 1.691 \pm 0.015$ and the cross-calibration factors are $K^{2012}_{\mathrm{A-B}} = 1.017 \pm 0.015$ and $K^{2013}_{\mathrm{A-B}} = 1.000 \pm 0.020$. If we leave the photon indices of the 2012 and 2013 observations free to vary independently, no improvement in the fit is found and they are both consistent with the inferred single best-fitting value. A neutral absorber along the line of sight does not improve the fit ($\Delta\chi^2 = 2$ for one additional variable parameter) and only an upper limit $N_\mathrm{H} < 8 \times 10^{22}$ cm^{-2} is found: this confirms that the circumnuclear absorbers in this object do not affect the analysis of the 10–80 keV *NuSTAR* spectra.

In the past, high-energy observations of NGC 2110 only revealed upper limits for the fraction R of the Compton reflection of the primary continuum by cold, neutral material (Malaguti et al. 1999; Rivers et al. 2014) which is usually found in Seyfert galaxies (Dadina 2008; Ricci et al. 2011). The addition of such a component in our fit, modelled with PEXRAV (Magdziarz & Zdziarski 1995) with Γ fixed to that of the primary continuum and the inclination angle to 60°does not lead to an improvement of the fit ($\Delta\chi^2 = 2$ for two additional variable parameters) and only upper limits $R_{2012} < 0.15$ and $R_{2013} < 0.14$ in the reflection components are found for the 2012 and 2013 observations, respectively. The contour plot between R_{2012} and Γ is shown in Fig. 1. Other parameters do not differ from the best-fitting values presented above. When we add a cutoff power law in our fit (model CUTOFFPL in XSPEC), no significant improvement is found ($\Delta\chi^2 = 2$ for one additional variable parameter): we find a best-fitting value of $\Gamma = 1.647^{+0.014}_{-0.053}$ and a lower limit $E_\mathrm{c} > 230$ keV for the cutoff energy.

[1] available at: http://www.asdc.asi.it/mmia/index.php?mission=saxnfi.

3.2 *NuSTAR* + *Swift* 3–80 keV spectral analysis

We then consider 2012 and 2013 *NuSTAR* data down to 3 keV and introduce the simultaneous *Swift*-XRT spectra, with net exposure times of 7.1 and 0.9 ks, respectively.

The model is composed of an absorbed power law with a high-energy cutoff and two Gaussian lines, to reproduce the Fe Kα and Kβ emission at 6.4 and 7.056 keV, respectively. We then convolved the baseline model with a Galactic column density $N_{\rm H}^{\rm G} = 1.62 \times 10^{21}$ cm^{-2} (Kalberla et al. 2005), modelled with TBABS in XSPEC, using solar abundances (Wilms, Allen & McCray 2000) and cross-sections from Verner et al. (1996). In XSPEC, the model reads as follows: TBABS*ZWABS*(CUTOFFPL+ZGAUSS+ZGAUSS). XRT-FPMA cross-calibration factors are introduced as a variable parameters. The fit is good (χ^2/dof=876/881=0.99) and no strong residuals are seen (Fig. 2).

The inclusion of Compton reflection in the fit leads to an insignificant improvement of the fit ($\Delta\chi^2 = 2$ for two additional variable parameters) and its contribution to the total 3–80 keV flux is $F_{\rm refl}^{2012} < 1.5$ per cent and $F_{\rm refl}^{2013} < 2.5$ per cent. Best-fitting cross-calibration factors are $K_{\rm XRT-FPMA}^{2012} = 0.98 \pm 0.03$ and $K_{\rm XRT-FPMA}^{2013} = 0.95 \pm 0.09$. We measure a lower limit for the high-energy cutoff $E_{\rm c} > 210$ keV and in Fig. 3, the contour plots of $E_{\rm c}$ versus Γ as well as $N_{\rm H}$ versus Γ are shown. Best-fitting values do not significantly differ from the ones discussed in Section 3.1.

We next use a more physical model (COMPTT in XSPEC; Titarchuk 1994) to measure the coronal temperature $kT_{\rm e}$ and optical depth τ. In this model, the soft seed photon spectrum is a Wien law; we fixed the disc temperature to 30 eV, appropriate for $M_{\rm BH} \approx 10^8$ M$_\odot$ (the black hole mass in NGC 2110 is estimated to be $M_{\rm BH} \sim 2 \times 10^8$ M$_\odot$ via the $M_{\rm BH}$–σ relation; Moran et al. 2007). In the case of a slab geometry, the fit is good (χ^2/dof=873/880 = 0.99) and best-fitting parameters $kT_{\rm e} = 190 \pm 130$ keV and $\tau = 0.22^{+0.51}_{-0.05}$ are found.

The measured iron Kα equivalent width (EW) for the 2012 and 2013 observations (EW$\simeq$35–200 eV, Table 2) are unusually large given the observed Compton reflection for the line to originate from reflection from Compton-thick material. We therefore confirm the result in Malaguti et al. (1999) from the low-flux *BeppoSAX* observation and with *Suzaku* (Reeves et al. 2006; Rivers et al. 2014). If the Compton reflection and the iron Kα emission line arise from the same distant, Compton-thick material, they can be self-consistently modelled using the PEXMON model in XSPEC (Nandra et al. 2007), with the inclination angle fixed at 60°. This leads to a best fit χ^2/dof = 930/884 = 1.06 with visible residuals around iron Kα. Leaving the iron abundance free to vary, a significant improvement in the fit is found ($\Delta\chi^2 = 34$ for one additional variable parameter) and we find a $A_{\rm Fe} > 22$ with respect to the solar value. No significant variation between photon index, reflection fraction, absorbing column densities, cross-calibration factors and best-fitting parameters discussed above is found. Such a large iron abundance is unrealistic, and therefore we discard this scenario.

The alternative scenario we consider is the one in which the line is produced by Compton-thin material ($N_{\rm H} = 10^{22}$–10^{23} cm^{-2}) that does not contribute significantly to the Compton reflection (Matt, Guainazzi & Maiolino 2003). We model the Compton reflection and

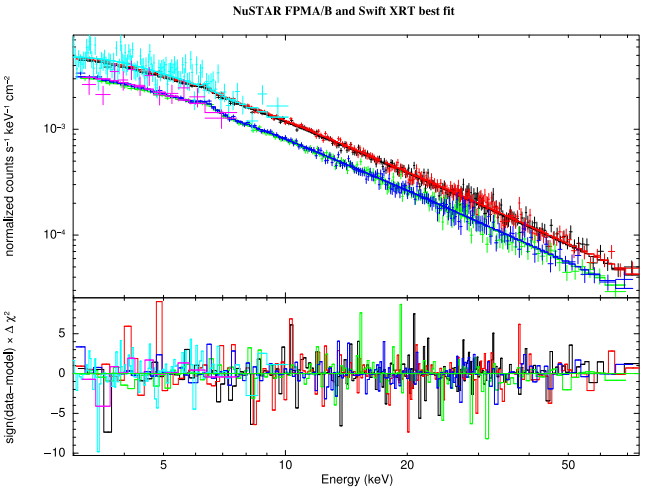

Figure 2. 3–80 keV simultaneous *NuSTAR*+*Swift* best fit. *NuSTAR* FPMA and FPMB spectra are in black and red for the 2012 observation, green and blue for the 2013 one. *Swift* XRT 2012 data are in light blue and 2013 spectra in magenta. Residuals are shown in the bottom panel, when a model composed of an absorbed cutoff power law and a Gaussian line at 6.4 keV is applied to our data set. No strong residuals are present across the whole energy band.

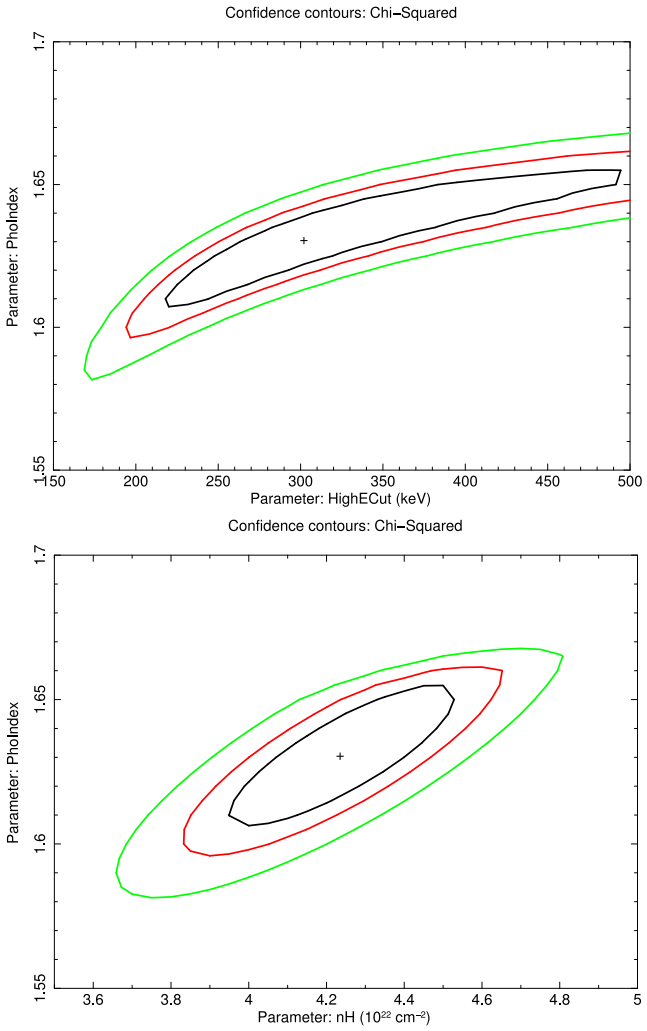

Figure 3. Top panel: contour plot between photon index Γ and cutoff energy $E_{\rm c}$, when simultaneous 3–80 keV *Swift*+*NuSTAR* data are considered. The solid black, red and green lines correspond to 68, 90 and 99 per cent confidence levels, respectively. High-energy cutoff values are limited to $\leq$500 keV because it is the maximum value allowed in the CUTOFFPL model. Bottom panel: contour plot between photon index Γ and absorbing column density along the line of sight.

Table 2. Best-fitting parameters when the 3–10 keV phenomenological fit is applied to the data. Column densities are in 10^{22} cm^{-2} units, energy centroids are in keV units, EW and widths (σ) of the Fe Kα line in eV units, line fluxes are in 10^{-5} ph cm^{-2} s^{-1} units and 3–10 keV observed fluxes are in 10^{-11} erg cm^{-2} s^{-1} units.

Instrument	Date	$N_{\rm H}$	Γ	Fe Kα En.	σ	EW	$F_{\rm K\alpha}$	$F_{\rm K\beta}$	$F_{\rm 3\text{-}10\,keV}$
BeppoSAX	1997-10-12	4.3 ± 0.9	1.74 ± 0.09	$6.43^{+0.06}_{-0.09}$	<280	194^{+69}_{-50}	$8.3^{+3.0}_{-2.3}$	<1.3	2.77 ± 0.05
Chandra	2001-12-19	4.0 ± 1.8	$1.67^{+0.30}_{-0.25}$	6.400 ± 0.008	16^{+14}_{-10}	90^{+30}_{-25}	$5.4^{+1.8}_{-1.5}$	<2.8	3.84 ± 0.07
Chandra	2003-03-05	<4.5	$1.25^{+0.48}_{-0.33}$	6.391 ± 0.016	30^{+31}_{-16}	135^{+60}_{-45}	$5.5^{+2.5}_{-2.0}$	<2.0	2.80 ± 0.07
XMM	2003-03-05	3.9 ± 0.4	1.57 ± 0.05	6.42 ± 0.01	62 ± 14	145 ± 15	5.0 ± 0.5	0.8 ± 0.3	2.26 ± 0.03
Suzaku	2005-09-16	3.8 ± 0.2	1.63 ± 0.02	6.40 ± 0.01	50 ± 15	55 ± 5	8.4 ± 0.8	0.6 ± 0.5	9.90 ± 0.03
Suzaku	2012-08-31	4.5 ± 0.2	1.63 ± 0.02	6.39 ± 0.01	<55	50 ± 7	9.7 ± 0.9	<1.0	11.8 ± 0.1
NuSTAR	2012-10-05	4.0 ± 0.4	1.64 ± 0.03	6.33 ± 0.07	<192	35 ± 10	9.5 ± 3.0	<2.3	17.1 ± 0.2
NuSTAR	2013-02-14	4.0 ± 0.7	1.64 ± 0.05	6.45 ± 0.07	175^{+200}_{-140}	90^{+42}_{-25}	$16.0^{+8.0}_{-4.0}$	<3.4	11.7 ± 0.2
				Swift best-fitting parameters					
χ^2/d.o.f.	Date	$N_{\rm H}$	Γ	Fe Kα En.	σ	EW	$F_{\rm K\alpha}$	$F_{\rm K\beta}$	$F_{\rm 3\text{-}10\,keV}$
59/61	2006-03-25	3.5 ± 2.5	1.35 ± 0.45	6.50 ± 0.15	115^{+80}_{-85}	190 ± 115	25.0 ± 15.0	<13	8.9 ± 0.5
83/85	2006-04-08	3.0 ± 2.0	1.25 ± 0.35	$6.50^{+0.11}_{-0.08}$	<250	100^{+80}_{-64}	$14.7^{+10.2}_{-9.3}$	<7	9.8 ± 0.5
15/24	2006-04-15	4.0 ± 2.3	1.7*	6.7 ± 0.5	<350	450^{+665}_{-400}	$50.9^{+78.5}_{-44.5}$	<34	8.1 ± 0.9
17/15	2008-08-31	7.5 ± 3.0	1.7*	6.4*	60*	<95	<9.0	<44	5.9 ± 0.9
37/35	2009-10-12	5.5 ± 3.5	$1.43^{+0.70}_{-0.51}$	6.2 ± 0.1	<350	170^{+120}_{-120}	35 ± 25	<38	11.4 ± 0.8
106/94	2012-10-05	5.9 ± 2.5	$1.7^{+0.3}_{-0.3}$	6.4*	60*	<35	<30.7	<15	17.3 ± 0.4
170/159	2013-02-03	6.3 ± 1.9	$1.75^{+0.25}_{-0.25}$	6.4*	60*	<50	<14	<13	16.0 ± 0.9
9/8	2013-02-15	7.0 ± 3.5	1.7*	6.4*	60*	<250	<53	<30	12.5 ± 1.6
81/56	2013-03-09	4.3 ± 1.2	1.7*	6.2 ± 0.1	60*	160 ± 100	22.7 ± 12.5	<10	8.0 ± 0.8

iron fluorescent lines with MYTORUS scattered and line components (Murphy & Yaqoob 2009; Yaqoob 2012). We add a further component to reproduce absorbing material along the line of sight. The assumed geometry is a torus of gas and dust with a 60°opening angle. When we apply this model to the 2012 and 2013 *Swift+NuSTAR* simultaneous data, we leave the normalization of the primary continua and the column density along the line of sight as variable parameters. Normalizations and column densities of the scattered and line components are linked and free to vary. The fit is good (χ^2/dof=907/884 = 1.02) and we find that no variations from best-fitting parameters discussed above are found. The best-fitting value for the column density of the scattering material producing the iron Kα is $N_{\rm H} = 2.0 \pm 1.1 \times 10^{23}$ cm^{-2}. The ratios between the scattered and primary components' normalizations are consistent with unity, the standard MYTORUS configuration (coupled reprocessor model in Yaqoob 2012), in which the torus is not aligned along the line of sight.

The value of the column density of the iron Kα emitting gas is consistent with the estimate presented in Bianchi et al. (2003, $N_{\rm H} \simeq 3 \times 10^{23}$ cm^{-2}) for the case of NGC 7213, where the authors assumed a broad-line region covering factor $f_{\rm c} = 0.35$, an EW $\simeq$ 100 eV and a photon index $\Gamma = 1.69$. This suggests that the two sources do indeed present similar features in the X-ray band.

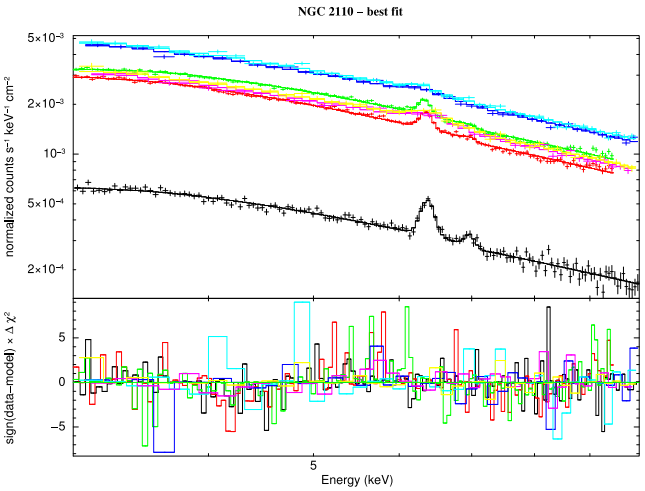

Figure 4. 3–10 keV phenomenological best fit. EPIC-Pn data are in black, *Suzaku* data from the 2005 and 2013 observations are in red and green, respectively. *NuSTAR* FPMA and FPMB data from the 2012 observation are in light and dark blue while *NuSTAR* FPMA and FPMB spectra obtained in 2013 are in orange and yellow, respectively.

3.3 Time history of the iron Kα line

We apply the model described in Section 3.2 (an absorbed primary continuum and two Gaussian lines) to the archival 3–10 keV data sets. This phenomenological fit is intended for studying the Fe Kα EW and flux on time-scales of months and years.

We first fit data with high SNR from *XMM–Newton*, *Suzaku* and *NuSTAR* with the above model: the fit is good (χ^2/dof=628/544=1.15) and no strong residuals are present across the energy band (Fig. 4). The best-fitting parameters are reported in Table 2. If we introduce a reflection component in our fit, no variation in the parameters of the lines is found with respect to the best-fitting values.

Then, we fit the 3–10 keV spectra of the nine *Swift* snapshots of the source, fixing the photon index to $\Gamma = 1.7$ (as inferred from the high-energy data analysis).Further parameters such as centroids and widths of the Fe Kα emission line are fixed to 6.4 keV and 60 eV (as inferred from the *XMM* and *Suzaku* analyses), respectively, where SNR was too poor to accurately measure these parameters. Best-fitting χ^2/dof values are reported in Table 2.

Fig. 5 shows the time evolution of the EW of the Fe Kα line flux and the observed 3–10 keV flux of the source. The object has a variable intrinsic emission in the 3–10 keV energy range: we

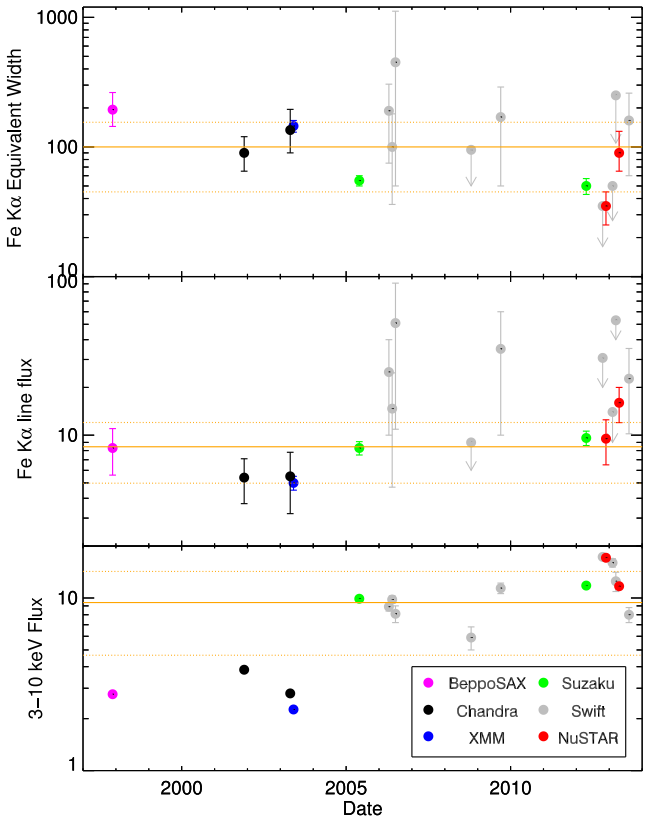

Figure 5. Time evolution of iron Kα parameters and 3–10 keV observed flux of the source (not corrected for absorption). EW are in eV units, line fluxes are in 10^{-5} ph cm^{-2} s^{-1} units and observed 3–10 keV fluxes in 10^{-11} erg cm^{-2} s^{-1} units. Solid and dashed horizontal lines represent mean and standard deviations, respectively.

measure a factor of $\sim$7.5 between the 2003 *XMM–Newton* and 2012 *NuSTAR* observations, while we find a factor of $\sim$ 1.5 between the *Swift* observation on 2013-02-03 and the *NuSTAR* observation on 2013-02-14 on a 10 d time-scale.

The variability of the Fe Kα emission line carries information about the distance and ionization state of the emitting material (width and energy centroid). Indeed, the measured Fe Kα flux in the 2003 *XMM* observation is significantly lower than the one measured with *Suzaku* three years later.

In Fig. 6, we plot Fe Kα fluxes and EW versus the observed 3–10 keV flux ($F^{\rm c}_{3-10}$), respectively. We examined the correlations between EW and $F^{\rm c}_{3-10}$ and between the Fe Kα flux and $F^{\rm c}_{3-10}$ by performing a linear fit using only high SNR observations (i.e. removing *Swift* data points).

We find a best-fitting relation EW $= (-8.2 \pm 1.6) \times F^{\rm c}_{3-10} + (163 \pm 20)$ with a Spearman's rank correlation coefficient $\rho = -0.88 \pm 0.06$ and a null-hypothesis probability of 5.5×10^{-3}. The other best-fitting relation is $F_{K\alpha} = (0.42 \pm 0.17) \times F^{\rm c}_{3-10} + (5.2 \pm 1.0)$ with a Spearman's rank correlation coefficient $\rho = 0.67 \pm 0.09$ and a null-hypothesis probability of 9.1×10^{-2}. Both best-fitting curves are shown in Fig. 6. When we introduce the *Swift* data points in the fit, we obtain less statistically significant relations, with null-hypothesis probabilities of 3.9×10^{-2} and 0.37 for the EW–$F^{\rm c}_{3-10}$ and $F_{K\alpha}$–$F^{\rm c}_{3-10}$ relations, respectively.

4 DISCUSSION

4.1 Properties of the hot corona

Recently, the *NuSTAR*'s high sensitivity above 10 keV has led to high-energy cutoff measurements in a number of nearby Seyfert galaxies: IC 4329A (178^{+74}_{-40} keV, Brenneman et al. 2014), SWIFT J2127.4+5654 (108^{+11}_{-10} keV, Marinucci et al. 2014), Ark 120 ($E_{\rm c} > 190$ keV; Matt et al. 2014) and 3C 382 (214^{+147}_{-63} keV; Ballantyne et al., 2014). The broad-band analysis of NGC 2110 presented in Section 3.1 leads to a lower limit on the high-energy cutoff,

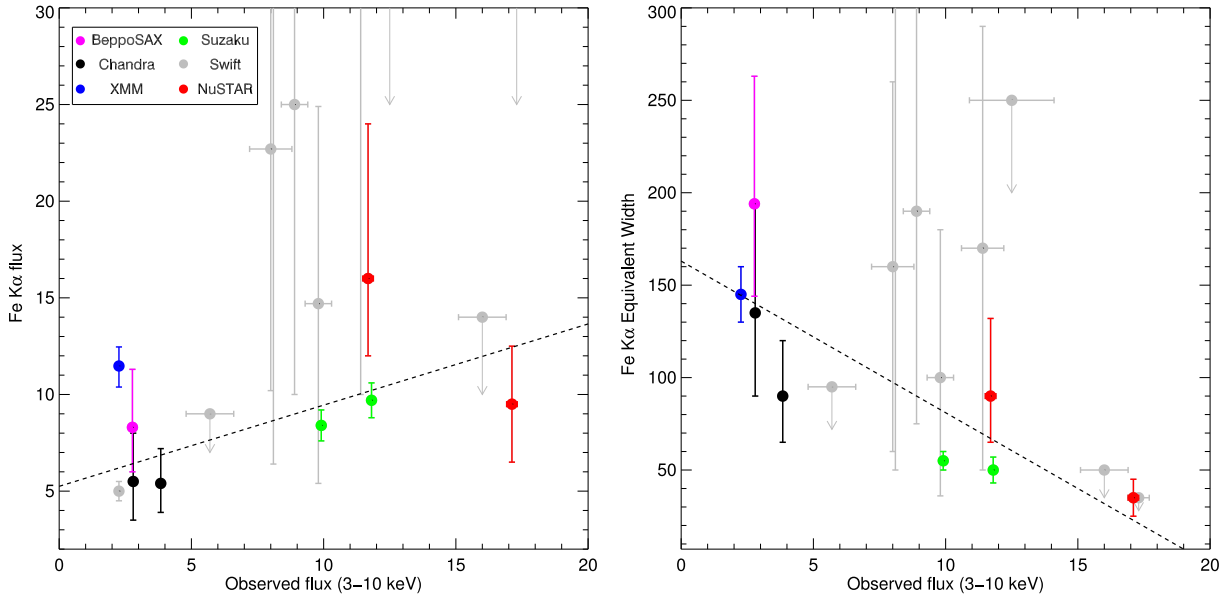

Figure 6. Left-hand panel*:* iron Kα flux (in 10^{-5} ph cm^{-2} s^{-1} units) plotted against intrinsic 3–10 keV flux (in 10^{-11} erg cm^{-2} s^{-1} units). Right-hand panel: iron Kα EW (in eV units) plotted against intrinsic 3–10 keV flux (in 10^{-11} erg cm^{-2} s^{-1} units). Dashed black lines represent best-fitting relations, when a linear fit is applied using only high SNR observations (i.e. removing *Swift* data points).

$E_c > 210$ keV. The unabsorbed 2–10 keV luminosity ranges within $L_X = 0.4–3.5 \times 10^{43}$ erg s^{-1} (considering the 2003 *XMM* and 2012 *NuSTAR* observations as low- and high-flux states, respectively). If we use the 2–10 keV bolometric corrections presented in Marconi et al. (2004), the bolometric luminosity ranges within $L_{bol} = 0.6–9 \times 10^{44}$ erg s^{-1}. A black hole mass of $M_{BH} \simeq 2 \times 10^8$ M$_\odot$ (Merloni, Heinz & di Matteo 2003; Moran et al. 2007) leads to an Eddington luminosity $L_{Edd} \simeq 2.4 \times 10^{46}$ erg s^{-1}. Therefore, for NGC 2110 we estimate $L_{bol}/L_{Edd} \simeq 0.25–3.7 \times 10^{-2}$. This value is at the lower end of the distribution recently measured in CAIXA (Catalogue of AGN in the XMM-Newton Archive) for a sample of 156 AGN (Bianchi et al. 2009a).

NGC 2110 is the second Seyfert galaxy kwown to unambiguously lack reprocessed emission from distant Compton-thick material and to show an iron Kα emission line likely produced by Compton-thin material. NGC 7213 is the other source known to have similar properties (Bianchi et al. 2003, 2008; Lobban et al. 2010). The latter is also accreting at a low Eddington rate ($L_{bol}/L_{Edd} \sim 3 \times 10^{-3}$) and Bianchi et al. (2008) reported a broad-line region origin for the iron Kα line. Interestingly, even though the two sources show remarkably similar spectral features in the X-rays, a high-energy cutoff $E_c = 95^{+50}_{-20}$ keV was detected in NGC 7213 in the simultaneous *XMM-BeppoSAX* data (Bianchi et al. 2004).

In the near future, more AGN will be observed by *NuSTAR* and we will be able to investigate the coronal properties (temperature, geometry, link to the reflected emission from the accretion disc) with greater detail in additional low accretion rate objects.

4.2 Iron Kα temporal behaviour

We analysed the 3–10 keV spectra of NGC 2110 from several X-ray observatories, spanning a period of 16 years. Large variations in the observed flux of the source and in the Fe Kα line flux and EW are apparent. If the Fe Kα line is produced by cold distant matter, we expect a constant line flux and an EW linearly anticorrelated with the intrinsic flux of the source. On the other hand, if the Fe Kα line-emitting material is closer than distances corresponding to the time-scales between the observations, we expect a constant EW and a line flux linearly correlated with the illuminating continuum. We instead find a correlation between the Fe Kα flux and the 3–10 keV observed flux $F_{K\alpha} \propto 0.42 \times (F^c_{3-10})$ and an anticorrelation between the Fe Kα EW and the 3–10 keV observed flux EW $\propto -8.2 \times (F^c_{3-10})$. We therefore propose a scenario where the Fe Kα line is the sum of two distinct components, one constant and produced from material distant from the nucleus (the putative 'torus') and the other one variable and linearly correlated with the primary flux that is likely associated with the broad-line region. In this scenario, the intercept of the relation between the Fe Kα flux and the 3–10 keV observed flux gives the amplitude of the constant component. We find a value of $(5.2 \pm 1.0) \times 10^{-5}$ ph cm^{-2} s^{-1}, perfectly consistent with the resolved *Chandra* component (Table 2). The Compton reflection fraction associated with this constant iron Kα component is consistent with the one found in the *NuSTAR* + *Swift* analysis (Section 3.2).

The emitting structure responsible for the variable component of the Fe Kα line, closer to the nucleus than the constant one, was discussed in Evans et al. (2007). These authors detected a modest broadening of the Fe Kα line in multi-epoch co-added High Energy Grating (HEG) spectra, with a line width $\sigma = 4500^{+3000}_{-2200}$ km s^{-1}. We speculate that this structure could be the same responsible for the broad, double-peaked Hα lines (FWHM $\sim$13 000–17 000 km s^{-1}) detected in optical spectro-polarimetric observations of this source (Moran et al. 2007; Tran 2010).

The *Astro-H* satellite, with its unprecedented combination of spectral resolution and collecting area at 6–7 keV, will allow us to resolve the iron line profile at 6.4 keV in NGC 2110 and determine the location of the circumnuclear emitting material and its Fe abundance.

4.3 A closer look to the circumnuclear environment

It is interesting to note that NGC 2110 appears to show features at infrared wavelengths arising from complex circumnuclear regions. If we consider the mid-infrared luminosity $L_{12\mu m} = 1.0 \times 10^{43}$ erg s^{-1} reported in Hönig et al. (2010) and the 2–10 keV luminosity range discussed above, NGC 2110 lies on the $L_{MIR} \propto (L_X)^{1.11}$ relation inferred in Gandhi et al. (2009), who analysed a sample of 42 Seyfert galaxies. This indicates that the geometry of the infrared emitter in NGC 2110 does not differ dramatically from other Seyfert galaxies. To produce enough IR continuum emission, the main requirement is enough dust with a sufficient covering factor to reprocess the intrinsic AGN power. This could be satisfied by a number of models, including a Compton-thin torus, or an extended dusty wind (Hönig et al. 2013, and references therein). In this way, one could potentially have strong dust emission, with very little accompanying X-ray Compton reflection.

In addition, NGC 2110 is one of the few Seyfert galaxies (together with NGC 7213) that also shows silicate dust features in emission (Hönig et al. 2010). The origin of silicate emission is not fully understood even in type 1 AGN, with non-standard dust grain properties, emission from a clumpy torus with a relatively small number of dust clumps, or emission from an extended dusty component in the narrow-line region, all invoked as possible sources (Sturm et al. 2005; Shi et al. 2006). Mason et al. (2009) discussed in detail such a feature and found that the mid-IR component in NGC 2110 cannot be extended more than 32 pc, ruling out extended reflecting clouds as seen in NGC 4945 (Marinucci et al. 2012). We conclude that a standard dusty torus/dusty wind model but with a gas column density in the Compton-thin regime could explain the X-ray and mid-IR characteristics of NGC 2110.

Beckmann & Do Cao (2010) reconstructed the spectral energy distribution of NGC 2110 using simultaneous *INTEGRAL* and *Swift* data taken in 2008 and 2009, reporting features usually shown by radio-loud sources. However, we do not confirm the flat photon index and cutoff energies they report. We use the radio fluxes at 6 cm ($F_{6cm} \simeq 165$ mJy; Griffith et al. 1995) and 20 cm ($F_{20cm} \simeq$ 300 mJy, Brown et al. 2011) and compare them with the 2–10 keV fluxes we found. No significant deviations from relations between radio and X-ray emission usually found in radio-quiet Seyferts are present (Panessa et al. 2007; Bianchi et al. 2009b, and references therein). Evans et al. (2006) analysed the *Chandra*, *HST* and *VLA* imaging observations and found a small radio jet (extended by $\sim$5″ accross the nucleus). However, the authors discarded the possibility of a synchrotron origin for the X-ray emission in NGC 2110, since the radio and X-ray emission are not spatially coincident.

5 SUMMARY AND CONCLUSIONS

We report a multi-epoch X-ray spectral analysis of the bright Seyfert 2 galaxy NGC 2110, spanning a period of 16 years. We focus on recent observations of the source with *NuSTAR* in 2012, when the source was at the highest flux level ever observed, and in 2013, when the source had more typical flux levels.

Our results can be summarized as follows.

(i) A high-energy cutoff $E_c > 210$ keV has been inferred, with an upper limit on the Compton reflection contribution of $R < 0.14$, confirming results from past high-energy *BeppoSAX* and *Suzaku* observations (Malaguti et al. 1999; Reeves et al. 2006; Rivers et al. 2014).

(ii) When multi-epoch data are considered, we find a correlation between Fe Kα EW and intrinsic 3–10 keV flux (EW $\propto -8.2 \times F^{c}_{3-10}$) and an anticorrelation between Fe Kα flux and intrinsic 3–10 keV flux ($F_{K\alpha} \propto 0.42 \times F^{c}_{3-10}$).

(iii) The Fe Kα line is likely the sum of two components: one constant (originating from distant Compton-thick material) and the other one variable and linearly correlated with the source flux (from matter at distances compatible with the broad-line region). Using MYTORUS self-consistent modelling, we find that the line could be produced by scattering material with a global covering factor of 0.5 with $N_H = 2.0 \pm 1.1 \times 10^{23}$ cm^{-2}.

(iv) The source presents remarkably similar features to the low accretion rate Seyfert 1 galaxy NGC 7213 in the X-ray band (lack of Compton reflection, contribution from Compton-thin material to the Fe Kα line emission) and in the infrared, where silicate dust emission was reported in Hönig et al. (2010).

ACKNOWLEDGEMENTS

AM and GM acknowledge financial support from Italian Space Agency under grant ASI/INAF I/037/12/0-011/13 and from the European Union Seventh Framework Programme (FP7/2007-2013) under grant agreement n.312789. This work was supported under NASA Contract No. NNG08FD60C, and made use of data from the *NuSTAR* mission, a project led by the California Institute of Technology, managed by the Jet Propulsion Laboratory, and funded by the National Aeronautics and Space Administration. We thank the *NuSTAR* Operations, Software and Calibration teams for support with the execution and analysis of these observations. This research has made use of the *NuSTAR* Data Analysis Software (NUSTARDAS) jointly developed by the ASI Science Data Center (ASDC, Italy) and the California Institute of Technology (USA).

MB acknowledges support from the International Fulbright Science and Technology Award.

REFERENCES

Arnaud K. A., 1996, in Jacoby G. H., Barnes J., eds, ASP Conf. Ser. Vol. 101, Astronomical Data Analysis Software and Systems V. Astron. Soc. Pac., San Francisco, p. 17
Ballantyne D. R. et al., 2014, ApJ. 794, 62
Beckmann V., Do Cao O., 2010, Proc. 8th Integral Workshop, The Restless Gamma-ray Universe, PoS(INTEGRAL 2010)081. Available at: http://pos.sissa.it/cgi-bin/reader/conf.cgi?confid=115
Bianchi S., Matt G., Balestra I., Perola G. C., 2003, A&A, 407, L21
Bianchi S., Matt G., Balestra I., Guainazzi M., Perola G. C., 2004, A&A, 422, 65
Bianchi S., La Franca F., Matt G., Guainazzi M., Jimenez Bailón E., Longinotti A. L., Nicastro F., Pentericci L., 2008, MNRAS, 389, L52
Bianchi S., Guainazzi M., Matt G., Fonseca Bonilla N., Ponti G., 2009a, A&A, 495, 421
Bianchi S., Bonilla N. F., Guainazzi M., Matt G., Ponti G., 2009b, A&A, 501, 915
Brenneman L. W. et al., 2014, ApJ, 781, 83
Brown M. J. I., Jannuzi B. T., Floyd D. J. E., Mould J. R., 2011, ApJ, 731, L41
Dadina M., 2008, A&A, 485, 417
Evans D. A., Lee J. C., Kamenetska M., Gallagher S. C., Kraft R. P., Hardcastle M. J., Weaver K. A., 2006, ApJ, 653, 1121
Evans D. A., Lee J. C., Turner T. J., Weaver K. A., Marshall H. L., 2007, ApJ, 671, 1345
Gabriel C. et al., 2004, in Ochsenbein F., Allen M. G., Egret D., eds, ASP Conf. Ser. Vol. 314, Astronomical Data Analysis Software and Systems (ADASS) XIII. Astron. Soc. Pac., San Francisco, p. 759
Gandhi P., Horst H., Smette A., Hönig S., Comastri A., Gilli R., Vignali C., Duschl W., 2009, A&A, 502, 457
George I. M., Fabian A. C., 1991, MNRAS, 249, 352
Griffith M. R., Wright A. E., Burke B. F., Ekers R. D., 1995, ApJS, 97, 347
Harrison F. A. et al., 2013, ApJ, 770, 103
Hayashi I., Koyama K., Awaki H., Yamauchi S. U. S., 1996, PASJ, 48, 219
Hönig S. F., Kishimoto M., Gandhi P., Smette A., Asmus D., Duschl W., Polletta M., Weigelt G., 2010, A&A, 515, A23
Hönig S. F. et al., 2013, ApJ, 771, 87
Jansen F. et al., 2001, A&A, 365, L1
Kalberla P. M. W., Burton W. B., Hartmann D., Arnal E. M., Bajaja E., Morras R., Pöppel W. G. L., 2005, A&A, 440, 775
Lobban A. P., Reeves J. N., Porquet D., Braito V., Markowitz A., Miller L., Turner T. J., 2010, MNRAS, 408, 551
Magdziarz P., Zdziarski A. A., 1995, MNRAS, 273, 837
Malaguti G. et al., 1999, A&A, 342, L41
Marconi A., Risaliti G., Gilli R., Hunt L. K., Maiolino R., Salvati M., 2004, MNRAS, 351, 169
Marinucci A., Risaliti G., Wang J., Nardini E., Elvis M., Fabbiano G., Bianchi S., Matt G., 2012, MNRAS, 423, L6
Marinucci A. et al., 2014, MNRAS, 440, 2347
Mason R. E., Levenson N. A., Shi Y., Packham C., Gorjian V., Cleary K., Rhee J., Werner M., 2009, ApJ, 693, L136
Matt G., Perola G. C., Piro L., 1991, A&A, 247, 25
Matt G., Guainazzi M., Maiolino R., 2003, MNRAS, 342, 422
Matt G. et al., 2014, MNRAS, 439, 3016
Merloni A., Heinz S., di Matteo T., 2003, MNRAS, 345, 1057
Moran E. C., Barth A. J., Eracleous M., Kay L. E., 2007, ApJ, 668, L31
Murphy K. D., Yaqoob T., 2009, MNRAS, 397, 1549
Mushotzky R. F., 1982, ApJ, 256, 92
Nandra K., Pounds K. A., 1994, MNRAS, 268, 405
Nandra K., O'Neill P. M., George I. M., Reeves J. N., 2007, MNRAS, 382, 194
Panessa F., Barcons X., Bassani L., Cappi M., Carrera F. J., Ho L. C., Pellegrini S., 2007, A&A, 467, 519
Piconcelli E., Jimenez-Bailón E., Guainazzi M., Schartel N., Rodríguez-Pascual P. M., Santos-Lleó M., 2004, MNRAS, 351, 161
Reeves J. N. et al., 2006, Astron. Nachr. 327, 1079
Ricci C., Walter R., Courvoisier T. J.-L., Paltani S., 2011, A&A, 532, A102
Rivers E. et al., 2014, ApJ, 786, 126
Rybicki G. B., Lightman A. P., 1979, Radiative Processes in Astrophysics. Wiley-Interscience, New York
Shi Y. et al., 2006, ApJ, 653, 127
Strüder L. et al., 2001, A&A, 365, L18
Sturm E. et al., 2005, ApJ, 629, L21
Titarchuk L., 1994, ApJ, 434, 570
Tran H. D., 2010, ApJ, 711, 1174
Turner M. J. L. et al., 2001, A&A, 365, L27
Verner D. A., Ferland G. J., Korista K. T., Yakovlev D. G., 1996, ApJ, 465, 487
Wilms J., Allen A., McCray R., 2000, ApJ, 542, 914
Yaqoob T., 2012, MNRAS, 423, 3360

This paper has been typeset from a TEX/LATEX file prepared by the author.